REPORT SSD-TR-90-04

Interdigitated Back Contact Silicon Solar Cell Analysis and Design Recommendations for Space Use

Prepared by

D. C. MARVIN and S. L. FROEDGE
Chemistry and Physics Laboratory
Laboratory Operations
The Aerospace Corporation
El Segundo, CA 90245

30 September 1989

Prepared for

SPACE SYSTEMS DIVISION
AIR FORCE SYSTEMS COMMAND
Los Angeles Air Force Base
P.O. Box 92960
Los Angeles, CA 90009-2960

This report was submitted by The Aerospace Corporation, El Segundo, CA 90245-4691, under Contract No. F04701-85-C-0086-P00019 with the Space Systems Division, P.O. Box 92960, Los Angeles, CA 90009-2960. It was reviewed and approved for The Aerospace Corporation by S. Feuerstein, Director, Chemistry and Physics Laboratory. Paul M. Propp was the project officer for the Mission-Oriented Investigation and Experimentation (MOIE) Program.

This report has been reviewed by the Public Affairs Office (PAS) and is releasable to the National Technical Information Service (NTIS). At NTIS, it will be available to the general public, including foreign nationals.

This technical report has been reviewed and is approved for publication. Publication of this report does not constitute Air Force approval of the report's findings or conclusions. It is published only for the exchange and stimulation of ideas.

PAUL M. PROPP, GM-14
MOIE Project Officer
SSD-WRDC-ML

RYMOND M. LEONG, MAJ, USAF
MOIE Program Manager
AFSTC/WCO OL-AB

UNCLASSIFIED

SECURITY CLASSIFICATION OF THIS PAGE

REPORT DOCUMENTATION PAGE

1a. REPORT SECURITY CLASSIFICATION Unclassified	1b. RESTRICTIVE MARKINGS
2a. SECURITY CLASSIFICATION AUTHORITY	3. DISTRIBUTION/AVAILABILITY OF REPORT Approved for public release; distribution unlimited.
2b. DECLASSIFICATION/DOWNGRADING SCHEDULE	
4. PERFORMING ORGANIZATION REPORT NUMBER(S) TR-0088(3945-01)-1	5. MONITORING ORGANIZATION REPORT NUMBER(S) SSD-TR-90-04
6a. NAME OF PERFORMING ORGANIZATION The Aerospace Corporation Laboratory Operations 6b. OFFICE SYMBOL *(If applicable)*	7a. NAME OF MONITORING ORGANIZATION Space Systems Division
6c. ADDRESS *(City, State, and ZIP Code)* El Segundo, CA 90245-4691	7b. ADDRESS *(City, State, and ZIP Code)* Los Angeles Air Force Base Los Angeles, CA 90009-2960
8a. NAME OF FUNDING/SPONSORING ORGANIZATION 8b. OFFICE SYMBOL *(If applicable)*	9. PROCUREMENT INSTRUMENT IDENTIFICATION NUMBER F04701-85-C-0086-P00019
8c. ADDRESS *(City, State, and ZIP Code)*	10. SOURCE OF FUNDING NUMBERS PROGRAM ELEMENT NO. / PROJECT NO. / TASK NO. / WORK UNIT ACCESSION NO.

11. TITLE *(Include Security Classification)*
Interdigitated Back Contact Silicon Solar Cell Analysis and Design Recommendations for Space Use

12. PERSONAL AUTHOR(S)
Marvin, Dean C. and Froedge, Sharon L.

13a. TYPE OF REPORT	13b. TIME COVERED	14. DATE OF REPORT *(Year, Month, Day)*	15. PAGE COUNT
	FROM _____ TO _____	1989 September 1989	30

16. SUPPLEMENTARY NOTATION-

17. COSATI CODES			18. SUBJECT TERMS *(Continue on reverse if necessary and identify by block number)*
FIELD	GROUP	SUB-GROUP	PISCES simulator, Electric Power Production, Power Supplies, Solar cells, Semiconductors (JG)

19. ABSTRACT *(Continue on reverse if necessary and identify by block number)* Interdigitated Back Contact

The Interdigitated Back Contact (IBC) solar cell is a relatively new design which has shown unprecedentedly high efficiencies. Silicon IBC cells have been fabricated that show greater than 25% efficiency at 100 suns Air Mass 1.5. This is far superior to conventional silicon concentrator cells which are approximately 18% efficient. The purpose of this report is to describe briefly the differences between this technology and conventional cells, demonstrate a near optimum design achieved by two-dimensional numerical simulation, and assess the utility of these cells for space application. The end of life (EOL) performance of this cell design in the radiation environment of space is a critical issue since the high efficiency of the design is predicated on the use of very high quality, long-diffusion length silicon. The radiation-induced degradation of this material is expected to lead to severe efficiency losses. The optimization of cell design to minimize these losses was carried out using a modified version of the 2-dimensional PISCES semiconductor simulator. The final designs presented here show that the performance of IBC cells in space can significantly exceed that of conventional cells.

20. DISTRIBUTION/AVAILABILITY OF ABSTRACT	21. ABSTRACT SECURITY CLASSIFICATION
☒ UNCLASSIFIED/UNLIMITED ☐ SAME AS RPT. ☐ DTIC USERS	Unclassified
22a. NAME OF RESPONSIBLE INDIVIDUAL	22b. TELEPHONE *(Include Area Code)* / 22c. OFFICE SYMBOL

DD FORM 1473, 84 MAR — 83 APR edition may be used until exhausted. All other editions are obsolete

SECURITY CLASSIFICATION OF THIS PAGE
UNCLASSIFIED

CONTENTS

FIGURES

TABLES

I. BACKGROUND

Silicon solar cells have served as the photovoltaic converters on virtually all DOD satellites. The state-of-the-art efficiency of these cells has risen from approximately 10% in the 1960s to nearly 15% Air Mass Zero (AM0) in the mid 1980s. The improvements in performance have been incremental during this period, resulting from the addition of such features as front and back surface field structures, back surface reflectors, and textured front surfaces. Each of these represents a modification of the solar cell; however, the basic structure of the solar cell has remained unchanged. It consists of a large area (several square centimeters) p-n junction, with a metal grid for the front face contact and complete metal coverage for the back contact. The features listed above are essentially modifications to the interfacial regions of the cell where much of the device physics occurs. In 1977 a group at Purdue University demonstrated 15% (AM1.3, 63 suns) efficiency and projected 20% (AM1.3, 300 suns) efficiency in radically redesigned solar cells,[1] named the Interdigitated Back Contact (IBC) solar cell. Further work at the University Louvain, Belgium, confirmed these findings. In 1987 researchers there fabricated IBC cells with demonstrated conversion efficiencies of 25.6% at 100 suns.[2]

The major difference between the IBC cell and a conventional cell is apparent in Fig. 1. In the IBC cell, the p-n junction is at the rear of the device (opposite the face where light enters) and consists of narrow strips under the contact metallization. This change carries with it a number of implications for device performance. The placement of the contact grid on the rear surface of the cell eliminates grid shadowing losses, which typically amount to 7-10%. Reduction of the junction area decreases the dark current, which in turn increases open circuit voltage (V_{oc}). Most light absorption occurs in a region doped much lower than a conventional cell emitter, resulting in much less recombination. Finally, the series resistance of this design is expected to be lower since the n^+ and p^+ contacts are close together, resulting in higher fill factors.

IBC Solar Cell

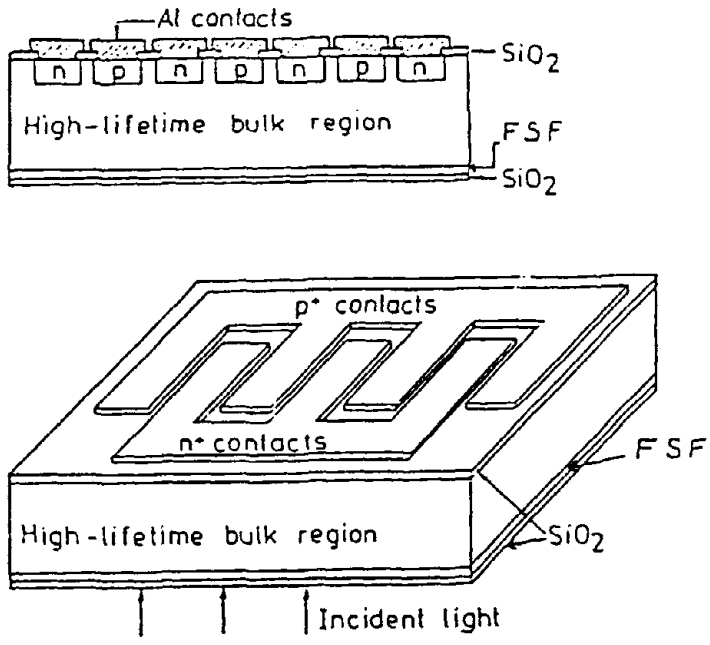

Conventional Solar Cell

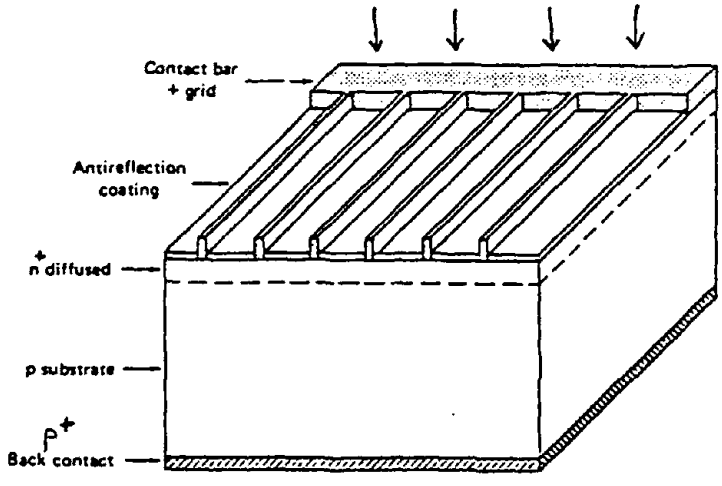

Fig. 1. Comparison of IBC Solar Cell with Conventional Point Contact Solar Cell

The Point Contact cell is similar in philosophy, but uses junction "islands" connected to contact grids rather than junction "lines" that are coincident with the metal grid. This further reduces the junction area but at the expense of added fabrication complexity. The predicted performances of the two designs are similar.

A primary concern about IBC cells in space applications is the expected sensitivity to radiation damage. The origin of the sensitivity is easily seen as follows. Light incident on the front surface of the cell is strongly absorbed in the first few micrometers of silicon, creating electron-hole pairs. These must diffuse through the entire thickness of the device without recombining in order to reach the doped contact regions which separate them at the rear of the cell. Thus, silicon with a minority carrier diffusion length of at least 100 um is typically required. This is no problem for present technology, except when the effects of electron irradiation are included. The damage caused by 1 MeV electron passage through the cell reduces the diffusion length substantially. For example, empirical results[3] on 10 ohm-cm silicon show an initial diffusion length of 700 um falls to 34 um after 1E15 1 MeV electron/cm^2 irradiation. A priori, one would therefore expect that cells of this design are unsuitable for high radiation environments.

The purpose of this study is to evaluate the IBC cell design for use in space missions. As described above the primary incentive for use of such cells is increased efficiency. This is especially true when the cells are operated under concentrated light. In order to properly simulate the operation of these cells, a two-dimensional solution of the carrier transport equations is necessary. This is in contrast to the situation with conventional cells where a one-dimensional treatment is often adequate. The distinction in treatments arises because of the localized nature of the p-n junction in the plane parallel to the front face in IBC cells. The study methodology is to vary the critical design parameters and simulate the cell current-voltage behavior at both the beginning and end of life under an assumed radiation environment. Basic IBC cell design parameters include base thickness and doping, contact region doping and dimensions, and front surface field (FSF) parameters. These are similar to the parameters in conventional

cells except for the additional degrees of freedom associated with the localized current collector regions, since in a conventional cell these cover the entire cell area on the front and rear faces.

II. THE PISCES SIMULATOR

The Poisson and Continuity Equation Solver (PISCES) computer code was developed at Stanford University. It is a true two-dimensional, two-carrier device modeling program. As supplied in Version IIb, the range of processes included is quite extensive. Fermi-Dirac carrier statistics, Auger and Shockley-Read-Hall (SRH) recombination, doping-induced band gap narrowing (BGN), and interface recombination are all treated. In addition, steady state and transient solutions are available. The program has been modified at Aerospace to include optical generation of carriers, thus allowing solar cell simulation. Optical generation functions for AM0 and AM1 light incident on silicon and gallium arsenide have been devised.

When used for absolute efficiency studies, as opposed to comparative studies, the accuracy of the generation function is important. In order to assess the accuracy of the AM0/silicon generation function, several simulations of IBC cells reported in the literature[4] were reproduced. These reports also used a two-dimensional simulator, along with all other processes included in PISCES, except for the use of Boltzmann instead of Fermi-Dirac statistics. The reported variation of IBC cell efficiency with cell thickness, illumination intensity, and interface recombination was investigated. It was necessary to normalize the PISCES results to the known intensity of AM0 light because the AM0/silicon generation function used in PISCES is not sufficiently accurate. This was done by computing the ratio of the known AM0 carrier generation in a given thickness of silicon[5] to the simulated short circuit current value obtained in the case of no recombination. All subsequent simulations of the same cell design were adjusted by this ratio, thus ensuring accurate absolute efficiencies. Having done this, the agreement in all cases tested was very good, not only with respect to relative variations, but also in the absolute sense.

III. RESULTS AND DISCUSSION

A. SCOPE OF THE STUDY

The purpose of this study is to evaluate the usefulness of Interdigitated Back Contact (IBC) solar cells in space applications. The scope of the study includes optimization of the IBC cell design under several different constraints and assessment of the effects of certain design parameters on cell performance. Since optimization is achieved by selecting parameters which produce the results desired to meet specific performance requirements, it is necessary to first understand how each parameter affects cell performance. Cell performance is assessed on the basis of overall cell efficiency η, maximum power P_{max}, short circuit current I_{sc}, open circuit voltage V_{oc}, fill factor FF, and collection efficiency. These are the parameters commonly used to judge solar cell performance, with perhaps the exception of collection efficiency. This quantity measures the fraction of photogenerated carriers which are ultimately delivered as current at the contacts. This is distinct from the cell efficiency which is defined as the fraction of incident optical power that is ultimately delivered as electrical power at the contacts. The collection efficiency is related to the overall cell efficiency through the open circuit voltage and fill factor.

A subset of all the possible design parameters was selected for study in order to have a manageable task. These include cell thickness, contact width, spacing and thickness, front surface field doping and thickness, and light intensity. The remaining parameters and constants were fixed at the values shown in Table 1. The baseline cell design is specified by the parameters in Table 2. These particular values were selected as representative of established silicon technology as applied to IBC structures. The carrier lifetime values for radiation scenario 1 are computed using a radiation degradation coefficient[6] obtained from a recent analysis of conventional silicon solar cell degradation. We regard these values as optimistic because they are extracted from experimental data by making certain unverified but reasonable assumptions. The assumed dose is 1E15 1 MeV electron/cm^2. Scenario 2 assumes

Table 1. Constant Cell Design Parameters

Electrode width	25 μm
p^+ doping concentration	5E18 cm^{-3}
n^+ doping concentration	5E18 cm^{-3}
p doping concentration	1.40E15 cm^{-3}
p Auger recombination	1.2E-31 cm^6s^{-1}
n Auger recombination	1.7E-31 cm^6s^{-1}
Hole mobility	475 cm^2/V^*s
Electron mobility	1380 cm^2/V^*s
Front surface recombination	1E3 cm/s
p^+/oxide recombination	1E4 cm/s
N^+/oxide recombination	1E6 cm/s
Metal contact resistance	0
Front surface reflectivity	0

Table 2. Basline Cell Design

p^+ width	35 μm
n^+ width	145 μm
p^+ thickness	1.0 μm
n^+ thickness	0.3 μm
p thickness	50 μm
τ_n in base	136 μs 1.10 μs[(a)] 0.32 μs[(b)]
τ_n in p^+ contact	0.128 μs 78 ns[(a)] 78 ns[(b)]
τ_p in n^+ contact	32.6 ns 12 ns[(a)] 12 ns[(b)]
FSF doping	5E18 p type
FSF thickness	0.5 μm

(a) After radiation scenario 1:
K_L = 2.5E-11 for p base
K_L = 1.10E-9 for p^+ region
K_L = 3.10E-8 for n^+ region

(b) After radiation scenario 2:
K_L = 8.40E-11 for p base
Other K_L s same as scenario 1.

the same dose, but with an experimentally obtained radiation degradation coefficient[3] for the base region. As pointed out in reference 6, this degradation coefficient is probably pessimistic because of the overly simplistic method by which it was obtained from the data. The second line of Table 3 shows that this baseline cell has a 1 sun efficiency of 14.87% BOL.

A COMSAT "Violet" cell was simulated to provide a basis for comparison with conventional silicon technology. A 250 μm thick cell of this type at 1 sun gave approximately 14.67% BOL and 13.2 EOL (under scenario 1) efficiency.

Subsequent sections present the effect on cell performance of variations about this baseline design. Cell performance at illuminations of 1 and 100 suns was calculated to evaluate systems with and without light concentration. All simulations were performed at 25°C.

B. CELL THICKNESS

Cell thickness effects are relatively simple to interpret. Thicker cells absorb a larger fraction of the incident light, especially the near-bandgap infrared, making the cell more efficient. However, the increased distance to the contacts means that a longer diffusion length is required and, therefore, higher quality silicon. The increased distance also means that thicker cells will be more susceptible to radiation-induced degradation.

Cells of 25, 50, and 200 micrometer thicknesses were simulated. The beginning of life (BOL) results in Table 3 show trends of increasing performance at 1 sun and decreasing performance at 100 suns as cell thickness is increased.

At 1 sun, efficiency increases by 1.4% (absolute) as cell thickness is increased from 25 to 200 μm. This increase is due to the additional absorption efficiency, which overcomes the decrease in collection efficiency arising from the extra diffusion distance that a thicker cell requires. The increased terminal current gives rise to a slight increase in V_{oc}.

At 100 suns, the BOL efficiency drops by 4.28% (absolute) as the cell thickness increases. In this case the higher carrier density throughout the

Table 3. BOL Effects of Cell Thickness

Cell Thickness	% η		P_{max} mWcm^{-2}		I_{sc} mAcm^{-2}		V_{oc} mV		% FF		% Collection Efficiency	
(μm)	1x	100x	1x	100x	1x	100x	1x	100x	1x	100x	1x	100x
25	13.67	15.26	18.54	20.60	42.59	47.09	541	662	80.10	66.08	99.76	99.53
50	14.87	14.31	20.07	19.31	45.47	49.79	548	680	80.54	57.04	99.49	99.03
200	15.06	20.98	20.33	14.82	47.34	47.35	548	676	78.36	46.30	95.08	87.07

cell causes the collection efficiency to decrease much more rapidly than in the 1 sun case. At first, this result seems contrary to the expectation that IBC cells are highly efficient under concentrated light. As is shown below, this baseline cell does not exhibit this behavior strongly because the contact regions are far from optimum.

The end of life (EOL) behavior following the more optimistic radiation scenario is shown in the upper part of Table 4. Clearly the thinnest cell has the best EOL performance, as expected. Also, each cell thickness shows little variation in EOL efficiency between 1 sun and 100 suns. The 25 μm cell has a 2% advantage over the 50 μm cell EOL for the baseline design at 1 sun. Table 4 shows the behavior of the 50 μm cell under the more realistic scenario 2 radiation. The loss of almost a factor of 2 in efficiency between the two radiation scenarios demonstrates the need for accurate radiation modeling input data, which may be obtained from experiments on bulk material rather than completed cells.

C. CARRIER COLLECTION REGION THICKNESS

The 50 μm thick cell was selected to study the effects of carrier collection region thickness.*

*BOL and EOL data are presented in Table 5. Trends observed in this cell were verified in simulations of the 25 μm thick cell, which are not presented here.

Table 4. EOL Effects of Cell Thickness

Cell Thickness (μm)	% η		P_{max} $mWcm^{-2}$		I_{sc} $mAcm^{-2}$		V_{oc} mV		% FF		P^+/N^+ Thickness (μm)	
	1x	100x	1x	100x	1x	100x	1x	100x	1x	100x		
25[1]	11.49	11.83	15.51	15.97	38.15	38.80	510	560	79.72	63.31	1.0	0.3
50[1]	9.49	9.88	12.81	13.33	32.37	37.86	502	646	78.84	54.51		
50[2]	5.05	5.32	6.82	7.18	18.77	19.70	482	600	77.78	60.80		
200[1]	1.00	1.05	1.33	1.41	3.93	3.46	443	560	76.48	72.89		
25[1]	11.98		16.18		38.53		526		79.82		3.0	0.9
50[1]	10.09		13.63		33.84		506		79.58			

[1] Radiation scenario 1.
[2] Radiation scenario 2.

Table 5. Effects of P^+ and N^+ Collection Region Thicknesses, BOL and EOL

Cell Thickness (μm)	% η		P_{max} $mWcm^{-2}$		I_{sc} $mAcm^{-2}$		V_{oc} mV		% FF		P^+/N^+ Thickness (μm)	
	1x	100x	1x	100x	1x	100x	1x	100x	1x	100x		
50	14.87	14.31	20.07	19.31	45.47	49.79	548	680	80.54	57.04	1.0	0.3
50[1]	9.49	9.88	12.81	13.33	32.37	37.86	502	646	78.84	54.51		
50	15.62	16.22	21.08	21.90	45.47	49.85	572	696	81.09	63.13	3.0	0.9
50[1]	10.09		13.63		33.84		506		79.58			
50	15.64		21.12		45.47		572		81.19		3.0	3.0

[1] EOL, radiation scenario 1.

At light intensities of 1 sun and 100 suns, BOL cell performance improvements in efficiency, P_{max}, V_{oc}, and FF were observed when respective p^+ and n^+ regions were changed from 1.0/0.3 μm to 3.0/0.9 μm thick, as shown in Table 5. Collection efficiency and I_{sc} remained constant as expected. There was no change in performance when the n^+ collection region thickness was further increased to 3.0 μm. The results thus indicate that an approximate 0.8% increase in BOL efficiency can be obtained by increasing the thickness of the doped contact regions.

The EOL figures included in Table 5 show that most of this 0.8% BOL improvement is retained at EOL. Therefore, the conclusion of this portion of the study is that doped contact regions which are thicker than those in the baseline design will improve both BOL and EOL performance.

D. CARRIER COLLECTION REGION WIDTH

The 50 μm baseline cell described in Table 2 was again selected for study of the effects of minority (n^+) and majority (p^+) carrier collection region widths. Since the baseline cell was near optimum for 1 sun, the overall cell efficiency was expected to decrease as the region widths were changed. However, an incremental decrease in the n^+ region width from 145 μm to 90 μm resulted in higher cell efficiencies as shown in Table 6. This increase in cell efficiency at first seems contrary to intuition since the minority carrier diffusion length of 700 μm (BOL) is sufficient for these carriers to reach the contact effectively irrespective of its size. One possibility is that the increased efficiency is due to the reduced n^+/oxide interface area, which results in lower interface recombination losses. However, the table shows that while the contact width is reduced, the collection efficiency is also decreasing. In fact, the increase in efficiency is due to an increased V_{oc} and fill factor. This can be understood by remembering that the dark current of the cell I_0, which is caused by carrier injection from the contacts into the base region, is reduced when the area of the contact/base interface is reduced. Since V_{oc} varies as $\ln(I_{sc}/I_0)$, an increased V_{oc} is expected. Although the efficiency only increases by 0.25% at 1 sun BOL, it can be more significant at EOL. At 100 suns the improvement is 4.3%. For this study we have not performed a detailed EOL optimization of a concentrator cell.

Table 6. Effects of P^+ and N^+ Collection Region Widths on 50 μm Thick Cell, BOL

% η		P_{max} mWcm^{-2}		I_{sc} mAcm^{-2}		V_{oc} mV		% FF		% Collection	P^+/N^+ Thickness
1x	100x	1x	100x	1x	100x	1x	100x	1x	100x	100x	(μm)
14.87	14.31	20.07	19.31	45.47	49.79	548	680	80.5	57.0	98.98	35/145
14.79		19.96		45.41		548		80.2			35/135
14.84	15.25	20.04	20.59	45.43	49.75	548	681	80.5	60.8		35/125
14.93	16.47	20.16	22.24	45.18	49.59	552	686	80.8	65.4	98.58	35/90
	17.54		23.68		49.45		681		70.3	98.30	60/90
14.90	18.40	20.10	24.84	45.10	49.42	551	684	80.9	73.4	98.23	90/90
15.12	18.76	20.41	25.32	45.09	49.23	560	693	80.8	74.2	97.86	90/70
15.00	18.73	20.24	25.29	44.90	49.21	560	692	80.5	74.3	97.81	90/50

E. ABRUPT FRONT SURFACE FIELD

The front surface field (FSF) is a heavily doped region, p^+ in the present case, which covers the entire front face of the solar cell. Its purpose is to provide an electric field that repels one carrier type away from the front surface. This effectively reduces the surface recombination velocity by reducing the concentration of one type of carrier near the surface. The FSF is generally introduced by heavier doping in a thin layer near the interface. This doping may be a step function, in which case it is often referred to as a minority carrier mirror, or a graded region. The graded region, although more difficult to tailor experimentally, is somewhat more effective since the field is present over the entire region thickness.

The effects of FSF thickness and doping level were studied for the base-line cell geometry at BOL. For thicknesses of 0.25, 0.5, and 1.0 μm at 1E18 doping, no significant effect was observed at 1 sun. The FSF effectiveness is relatively constant over a rather broad range around 1E17 to 1E18 cm^{-3}, decreasing below this level due to the weakness of the electric field and decreasing above this level due to increased Auger recombination. As will be shown in the next section, the FSF doping level becomes very important for a graded FSF.

F. DESIGN REFINEMENTS

Using the baseline cell as a starting point, the IBC cell design has been investigated to show how the parameters should be varied to produce an optimum design for various applications. In cases where radiation exposure is not present as the result of shielding or terrestrial use, the 1 sun cell should be at least 50 μm thick, have contact doping widths approximately 90 μm for both minority and majority carriers with 20 μm spacing, and have doping thicknesses approximately 1 μm and 3 μm, respectively. The efficiency of this cell will be near 16% AMO. A 100 sun cell will be very similar but will have an efficiency near 20%.

For space use, where radiation is present, EOL performance must be considered. The baseline cell parameters are near optimum for EOL efficiency. One method of further optimizing for EOL performance is by reducing cell thickness to 25 μm and increasing the contact doping region thickness. The gain in EOL efficiency will be nearly 2% at both 1 sun and 100 suns as the cell is thinned from 50 μm to 25 μm. Thus, the improvement over the baseline cell at 1 sun and 100 suns under these conditions is a total of 2.5%, with 2% attributable to cell thinning and 0.5% to contact doping thicknesss.

Recognizing that silicon cells as thin as 25 μm represent a major challenge in fabrication, we have investigated whether this excellent EOL performance can be obtained in a more conventional 50 μm thick cell. The additional design variations which we consider are the collector region spacing, the use of a graded front doping, and the bulk silicon/oxide back surface passivation. The previous results considered recombination only at the collector/oxide interfaces, which has been shown to be less important than the bulk/oxide interface. The results presented below indicate that if the latter interface can be well passivated (S<1E3 cm/sec), high EOL efficiency can be maintained in a thicker cell.

The initial parameter variation aimed at re-optimizing the structure consisted of decreasing the collector spacing from 20 μm to 10 μm. This increased the EOL efficiency from 10.1% to 10.3%. This change does not increase the metal grid coverage on the cell--it only changes the arrangement

of the doping regions underlying the metal grid. Even if the interface between these doping regions and the oxide surface is poorly passivated (S = 1E4 cm/sec) this performance can be achieved. This result and that reported previously assume excellent passivation (S < 10 cm/sec) of the bulk/oxide interface between the doping regions. For comparison, the 25 μm cell with 20 μm spacing gave 11.98% EOL efficiency. Thus, changes in contact spacing alone are not sufficient to regain the EOL efficiency lost in going to a 50 μm thickness from 25 μm.

In order to regain more of the performance lost by doubling the cell thickness from 25 μm to 50 μm, the use of a graded front surface doping field was investigated. The previous design used a 0.5 μm thick front surface field (FSF) uniformly doped at 5E18. It was found that by replacing this with a Gaussian doping profile with a characteristic width of 15 μm and a peak concentration of 1E18, the EOL efficiency was 11.49% with a 10 μm collector region spacing. This feature restored most of the lost performance. Table 7 shows the effects of a graded FSF with characteristic length of 15 μm as a function of doping level (peak concentration ranges from 5E16 to 5E18).

However, the importance of the bulk/oxide passivation is greatly increased when graded FSF is used. In the ungraded FSF 50 μm cell reported previously, the EOL efficiencies are 10.1% and 9.77% for recombination velocities at this interface of 0 and 1E4 cm/sec, respectively. For the graded design studied here, the corresponding efficiencies are 11.49% and 7.2%. Thus the improved efficiency of the graded structure carries with it the requirement of good surface passivation. Figures 2 and 3 show how the carrier flow differs between the unpassivated (high recombination, Fig. 2) and passivated (low recombination, Fig. 3) cases. In each figure a portion of the simulated cell is shown. The large minority collector (n^+) is shown in the upper left corner and a fraction of the smaller majority collector (p^+) is in the upper right corner. The figures show a 20 μm thick portion of the cell. Thus the important bulk/oxide interface between the two collector regions is featured. The line segments in each figure are vectors whose length represents the minority carrier (electrons in this case, since the base region is p type) current at a particular point in the cell and whose orientation shows

Table 7. Efficiency as a Function of FSF for 50 μm Cell at 1 Sun

Graded FSF to 15 μm	Step FSF 0.5 μm	FSF Doping cm^{-2}	% Cell Efficiency BOL	EOL
X		5E16	15.09	12.12
X		1E17	15.07	12.30
X		5E17	14.56	12.09
X		1E18	13.98	11.49
X		3E18		9.29
X		5E18		7.66
	X	5E18		10.29

the current flow direction. In both figures the light is incident from below. Addressing the high recombination case first, observe the fate of electrons generated on the left side of the figure. In order to contribute to the cell output current, these electrons must reach the minority collector in the upper right corner of the figure. The current vectors show, however, that some current flows to the left around the majority collector, resulting in recombination at the bulk/oxide interface. A larger current flows around the right side of the majority contact and results in significant recombination at the interface between the two collectors. Electrons generated on the right side of the figure (near 60 and 70 μm) do succeed in reaching the minority collector. The interface losses shown in this figure explain the poor performance of the graded field cell when surface passivation is inadequate.

Now considering the low recombination figure, it is seen that even electrons generated on the left side of the figure are directed around the majority collector to the right so that they subsequently reach the minority collector. None of the vectors show currents directed toward the interfaces. Thus this cell has much higher efficiency. The added sensitivity of the graded doping cell to surface recombination probably arises from the doping-induced drift field which drives the minority carriers toward the rear of the

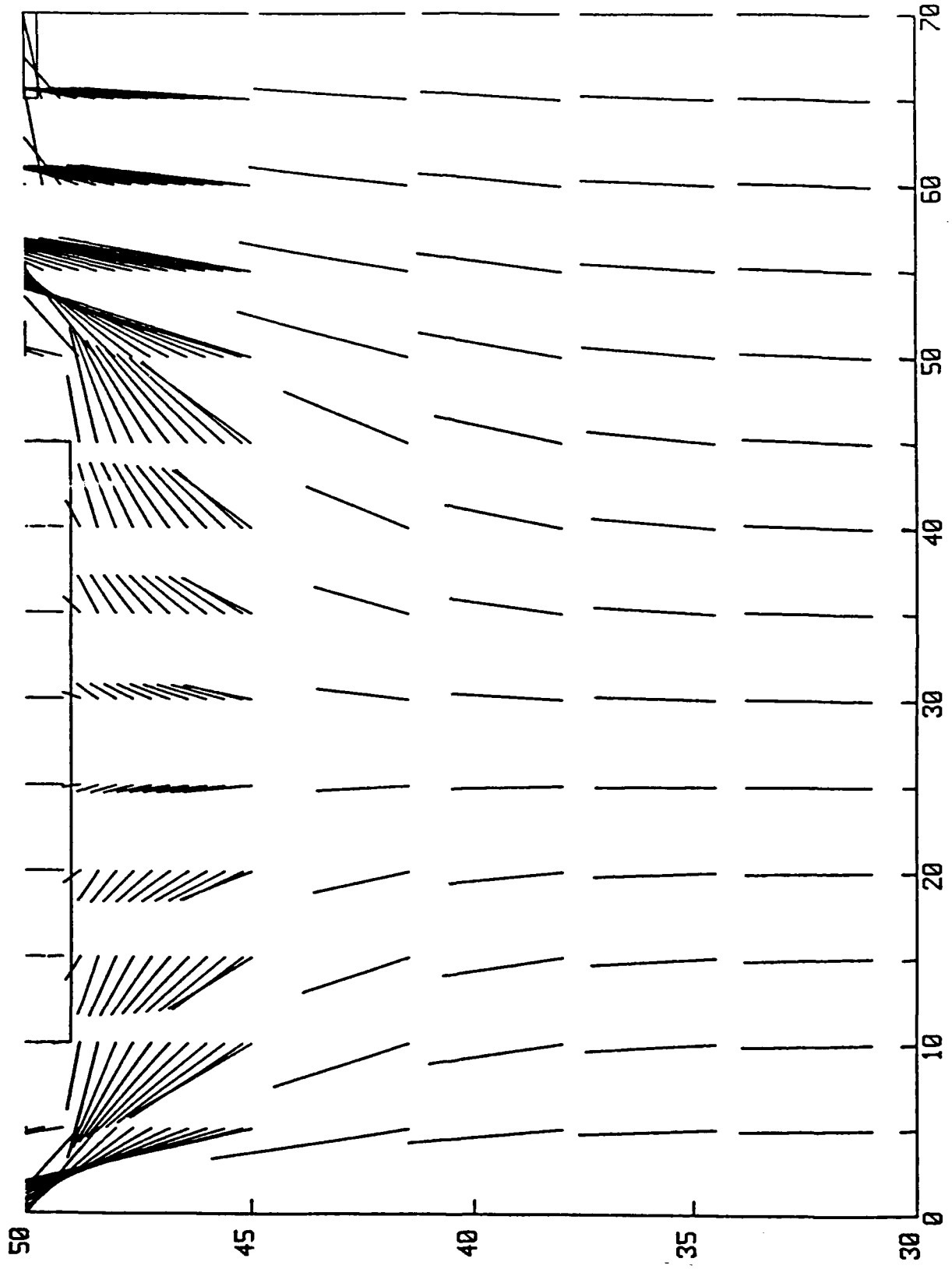

Fig. 2. Carrier Flow in High Recombination Case

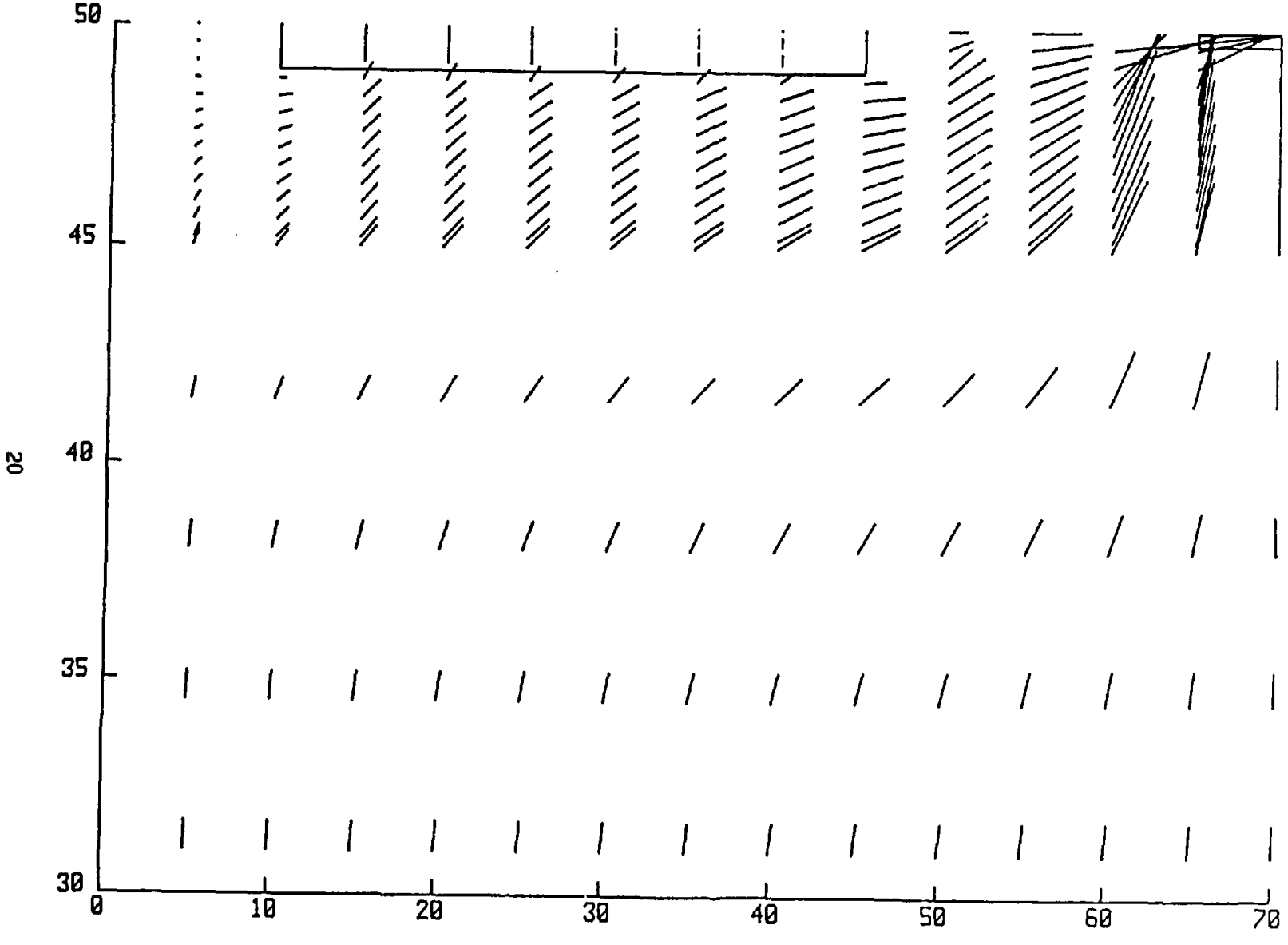

Fig. 3. Carrier Flow in Low Recombination Case

cell, rather than allowing them to diffuse toward the minority collector. Therefore, they are more likely to encounter the surface regions where recombination occurs.

Thus, the best 1 sun EOL performance is obtained with the 25 μm thick cell (11.98%), but a reasonable approximation of this can be obtained in a 50 μm cell (11.49%) with a graded front surface field with characteristic length approximately 15 μm and peak concentration roughly 1E18, combined with good interface control at the bulk/oxide interfaces.

Since breakage can be a significant problem for silicon cells 50 μm or less in thickness, we have made a study of 65 and 80 μm thicknesses which offer added mechanical strength at some expense of EOL efficiency. The attached graph (Fig. 4) shows the results.

The + signs represent cells with the 15 μm graded front surface field (FSF), 10 μm contact doping region spacing, 3 μm thick p^+ regions, and 0.9 μm thick n^+ regions. These parameters are identical to those for the optimized design reported previously. The loss in EOL efficiency in going from 50 to 80 μm is seen to be greater than 2%. The degradation assumed scenario 1 as described previously. The * signs represent cells with the same graded FSF but assuming the more pessimistic scenario 2 degradation. The change in efficiency is again near 2%, and is therefore roughly independent of the degradation scenario used.

For comparison, the effect of thickness on cell efficiency when a more conventional step front surface field is used is shown with the symbol X. The solid line portion of this graph is for cells of the same design as those just described except with a 0.5 μm thick FSF instead of the graded FSF. The two X symbols connected by the dashed line have the additional difference that the contact doping region spacing is 20 μm instead of 10 μm. These additional points are included simply to show how the trend extends to 25 μm.

The conclusion of this analysis on cell thickness is that both FSF cell designs suffer significant 1 sun EOL efficiency loss as the cell thickness increases from 50 to 80 μm, and that the amount of loss is roughly the same. Thus the graded FSF design retains its 2% efficiency advantage over the step FSF design under these conditions.

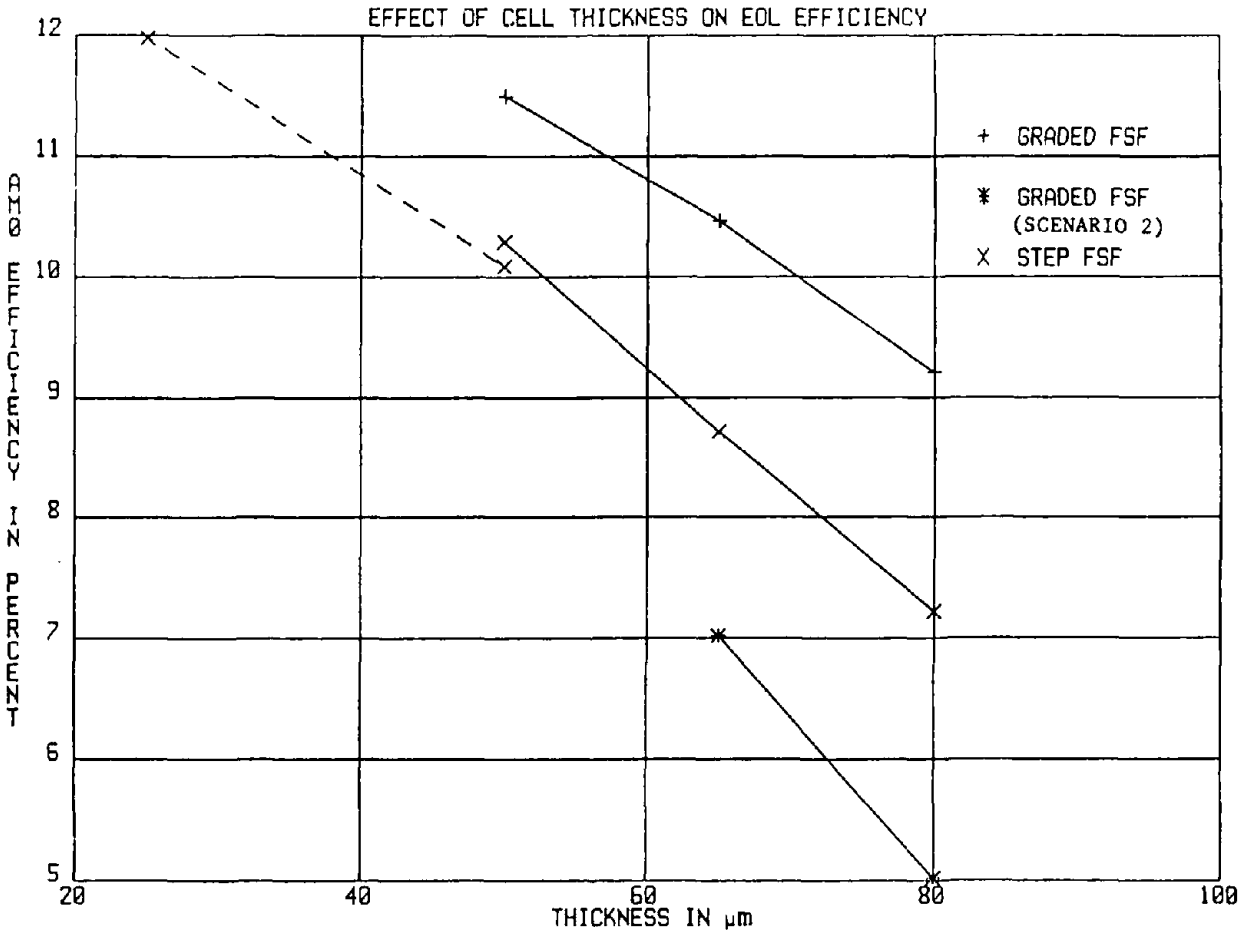

Fig. 4. Effect of Cell Thickness on EOL Efficiency

G. CONCENTRATED LIGHT LEVELS

IBC solar cells are designed to take advantage of concentrated light levels. Under concentration they are far superior to conventional cells in efficiency. Operation at 1 sun does not offer BOL efficiencies that significantly exceed those achievable with conventional designs. Therefore, simulations at 100 suns were performed to see whether or not the same optimum design rules applied at concentrated light levels. BOL efficiency for the 1 sun optimized design described above was approximately 18% at 100 suns. When the FSF was graded to 5 μm instead of 15 μm, BOL efficiency was about 16.6%.

Cell thicknesses of 50, 65, 80, and 200 micrometers were simulated at 100 suns using the near-optimal design parameters described above. We found that the 15.44% EOL efficiency for a 50 μm thick cell with this design is comparable to that of GaAs space cells. A 65 μm thick cell has an EOL efficiency of 11.57%. Table 8 summarizes the results of increased cell thickness at 100 suns for the optimum design. Included in Table 8 are results of increased cell thickness at 100 suns with the nonoptimum step FSF.

Table 8. EOL Efficiency as a Function of cell Thickness and FSF at 100 Suns

Cell Thickness (μm)	Graded FSF (μm)	Step FSF (μm)	FSF Doping cm^{-3}	*Spacing a/b/c	Cell Efficiency (%)
50	15	—	1E18	10/20/10	14.64
50	15	—	1E18	5/10/5	15.44
65	15	—	1E18	5/10/5	11.57
80	15	—	1E18	5/10/5	8.97
200	15	—	5E18	5/10/5	1.18
65	—	0.5	5E18	5/10/5	8.17
80	—	0.5	5E18	5/10/5	6.83

*a,c = spaces between right and left edges of collectors and unit cell boundaries, resp.; b = space between collectors. All dimensions are in micrometers.

The 18% BOL efficiency of the 1 sun optimized cell is significantly lower than the 25% efficiency quoted in Section I for two reasons. First, the present figure is for AM0 illumination rather than AM1.3. For conventional cells this difference in spectrum leads to a 2-3% decrease (absolute) in efficiency. Second, the baseline design is intended for 1 sun operation whereas the cell referred to earlier is intended for and operated at several hundred suns. The BOL efficiencies of the cells described in Table 8 were not calculated for comparison with the 25% frame in Section I because these cells are optimized for EOL efficiency, while the 25% cell is optimized for BOL.

IV. CONCLUSION

The design of IBC solar cells for space use has been investigated using 2-dimensional computer simulations. Near-optimal designs have been presented for missions using either planar or 100 sun concentration for arrays, under high or negligible radiation fluences. In the low radiation environment, the minority and majority carrier collection regions should be of comparable width, with thicknesses of 0.9 μm and 3.0 μm, respectively. The FSF should be an approximately 0.5 μm step with doping concentration of 5E18 cm^{-3}. These parameters are much more critical for 100 sun operation. The 1 sun efficiency of IBC cells exceeds 15%, which makes them competitive with conventional design silicon cells. The 100 sun efficiency is nearly 19%, which greatly exceeds the conventional silicon cell capability. It is also in the expected efficiency range of GaAs concentrator cells, although the operating temperature of each is quite important in comparing efficiencies.

In a high radiation environment, a different design is used to maximize the EOL performance. At 1 sun after 1E15 1 MeV electron fluence, the design presented here shows over 12% efficiency. The carrier collection region widths in this design are in an approximately 4 to 1 ratio, unlike the low radiation case. The FSF is graded over 15 μm with a peak doping concentration of 1E17 to 1E18 cm^{-3}. At 100 suns the EOL efficiency approaches 16%, which is comparable to that expected for GaAs concentrator systems. The high radiation environment cell design is summarized in Table 9. The effect of proton irradiation has not been addressed here, but the very deep junction should lead to high resistance to low energy front side proton irradiation.

The overall conclusion of this study is that properly designed IBC cells can yield performance which is comparable with (or superior to) competing silicon and gallium arsenide technologies. Therefore, their use in space systems should be considered. It is especially important with IBC cells to optimize the design to the particular mission profile. The light intensity to be used and the radiation environment affect the design to a greater extent than in conventional cells.

Table 9. High-Radiation Environment Cell Design Parameters

Electrode width	25 μm
p^+ doping concentration	5E18 cm^{-3}
n^+ doping concentration	5E18 cm^{-3}
p doping concentration	1.40E15 cm^{-3}
p Auger recombination	1.2E–31 cm^6s^{-1}
n Auger recombination	1.7E–31 cm^6s^{-1}
Hole mobility	475 $cm^2/V*s$
Electron mobility	1380 $cm^2/V*s$
Front surface recombination	1E3 cm/s
p^+/oxide recombination	1E4 cm/s
n^+/oxide recombination	1E6 cm/s
Metal contact resistance	0
Front surface reflectivity	0
p^+ width	35 μm
n^+ width	145 μm
p^+ thickness	1.0 μm
n^+ thickness	0.3 μm
p thickness	50 μm
τ_n in base	136 μs 1.10 μs[a] 0.32 μs[b]
τ_n in p^+ contact	0.128 μs 78 ns[a] 78 ns[b]
τ_n in n^+ contact	32.6 ns 12 ns[a] 12 ns[b]
FSF doping (peak concentration)	1E17 p type
Gaussian width	15 μm

(a) After radiation scenario 1:
K_L = 2.5E–11 for p base
K_L = 1.10E–9 for p^+ region
K_L = 3.10E–8 for n^+ region

(b) After radiation scenario 2:
K_L = 8.40E–11 for p base
Other K_Ls same as scenario 1.

REFERENCES

1. M. D. Lammert and R. J. Schwartz, IEEE Electron Devices Transcripts, ED-24, 337 (1977).

2. P. Verlinden et al, 19th Photovoltaic Specialists Conference Proceedings, New Orleans, LA (1987), p. 405.

3. Jet Propulsion Laboratories, Solar Cell Radiation Handbook, pp. 3-27 (1982).

4. D. J. Chin and D. H. Navon, Solid State Electronics, 24, 109 (1981).

5. H. J. Hovel, "Solar Cells", Vol. 11 of Semiconductors and Semimetals, Eds. Willardson and Beer, Associated Press, New York (1975).

6. G. F. J. Garlick and J. A. Minahan, 18th Photovoltaic Specialists Conference Proceedings, Las Vegas, NV (1985), p. 669.

LABORATORY OPERATIONS

The Aerospace Corporation functions as an "architect-engineer" for national security projects, specializing in advanced military space systems. Providing research support, the corporation's Laboratory Operations conducts experimental and theoretical investigations that focus on the application of scientific and technical advances to such systems. Vital to the success of these investigations is the technical staff's wide-ranging expertise and its ability to stay current with new developments. This expertise is enhanced by a research program aimed at dealing with the many problems associated with rapidly evolving space systems. Contributing their capabilities to the research effort are these individual laboratories:

Aerophysics Laboratory: Launch vehicle and reentry fluid mechanics, heat transfer and flight dynamics; chemical and electric propulsion, propellant chemistry, chemical dynamics, environmental chemistry, trace detection; spacecraft structural mechanics, contamination, thermal and structural control; high temperature thermomechanics, gas kinetics and radiation; cw and pulsed chemical and excimer laser development including chemical kinetics, spectroscopy, optical resonators, beam control, atmospheric propagation, laser effects and countermeasures.

Chemistry and Physics Laboratory: Atmospheric chemical reactions, atmospheric optics, light scattering, state-specific chemical reactions and radiative signatures of missile plumes, sensor out-of-field-of-view rejection, applied laser spectroscopy, laser chemistry, laser optoelectronics, solar cell physics, battery electrochemistry, space vacuum and radiation effects on materials, lubrication and surface phenomena, thermionic emission, photosensitive materials and detectors, atomic frequency standards, and environmental chemistry.

Computer Science Laboratory: Program verification, program translation, performance-sensitive system design, distributed architectures for spaceborne computers, fault-tolerant computer systems, artificial intelligence, microelectronics applications, communication protocols, and computer security.

Electronics Research Laboratory: Microelectronics, solid-state device physics, compound semiconductors, radiation hardening; electro-optics, quantum electronics, solid-state lasers, optical propagation and communications; microwave semiconductor devices, microwave/millimeter wave measurements, diagnostics and radiometry, microwave/millimeter wave thermionic devices; atomic time and frequency standards; antennas, rf systems, electromagnetic propagation phenomena, space communication systems.

Materials Sciences Laboratory: Development of new materials: metals, alloys, ceramics, polymers and their composites, and new forms of carbon; nondestructive evaluation, component failure analysis and reliability; fracture mechanics and stress corrosion; analysis and evaluation of materials at cryogenic and elevated temperatures as well as in space and enemy-induced environments.

Space Sciences Laboratory: Magnetospheric, auroral and cosmic ray physics, wave-particle interactions, magnetospheric plasma waves; atmospheric and ionospheric physics, density and composition of the upper atmosphere, remote sensing using atmospheric radiation; solar physics, infrared astronomy, infrared signature analysis; effects of solar activity, magnetic storms and nuclear explosions on the earth's atmosphere, ionosphere and magnetosphere; effects of electromagnetic and particulate radiations on space systems; space instrumentation.